Nanoporous Cathodes for High-Energy Li–S Batteries from Gyroid Block Copolymer Templates

Soumyadip Choudhury,[†,⊥] Mukesh Agrawal,[*,†,‡,⊥] Petr Formanek,[†] Dieter Jehnichen,[†] Dieter Fischer,[†] Beate Krause,[†] Victoria Albrecht,[†] Manfred Stamm,[†,§] and Leonid Ionov[*,†]

[†]Leibniz-Institut für Polymerforschung Dresden e.V., Hohe Straße 6, D-01069 Dresden, Germany and [§]Physical Chemistry of Polymer Materials, Technische Universität Dresden, D-01062 Dresden, Germany. [⊥]Soumyadip Choudhury and Mukesh Agrawal contributed equally to this work. [‡]Present address: SABIC Technology Center, Bangalore, India.

ABSTRACT

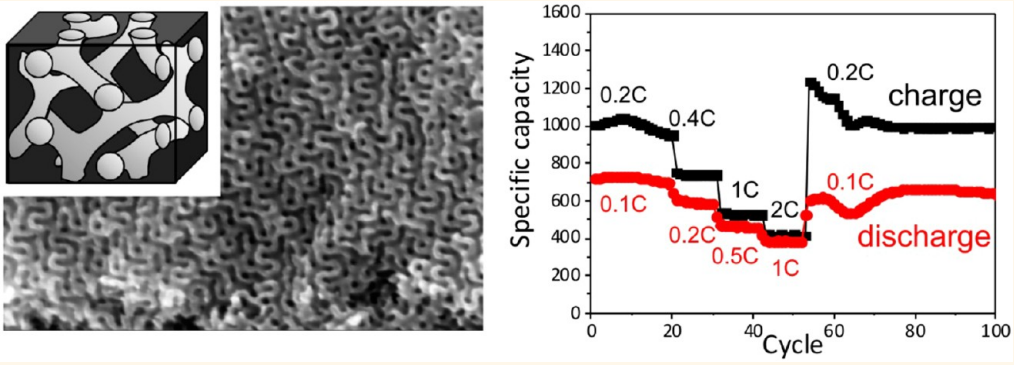

This study reports on a facile approach to the fabrication of nanoporous carbon cathodes for lithium sulfur batteries using gyroid carbon replicas based on use of polystyrene-poly-4-vinylpyridine (PS-P4VP) block copolymers as sacrificial templates. The free-standing gyroid carbon network with a highly ordered and interconnected porous structure has been fabricated by impregnating the carbon precursor solution into the gyroid block copolymer nanotemplates and subsequently carbonizing them. A wide range of analytical tools have been employed to characterize fabricated porous carbon material. Prepared nanostructures are envisioned to have a great potential in myriad areas such as energy storage/conversion devices owing to their fascinating morphology exhibiting high surface area and uniform porosity with interconnected three-dimensional networks. The resulting carbon nanoporous structures infused with elemental sulfur have been found to work as a promising electrode for lithium sulfur batteries demonstrating a high cycling stability over more than 200 cycles.

KEYWORDS: block copolymer · template · carbon · lithium–sulfur batteries · cathode

Ordered mesoporous materials have attracted immense interest from researchers for their applications in a wide range of areas ranging from heterogeneous catalysts, environmental technology, host–guest chemistry, and absorbents to energy storage (supercaps, Li-ion and Li–S batteries) because of their large specific surface area, uniform pore size distribution, tunable porosity, and well-defined surface properties.[1−6] Among them, a great deal of the research has been done on mesoporous elemental carbon materials, which are known to exhibit a unique combination of chemical, mechanical, electrical, and biocompatible properties.[7] They are widely being used in myriad application areas including nanoelectronic devices, strength-enhancing materials, separation media, catalyst supports, energy storage/conversion systems (hydrogen storage, fuel cell electrodes, *etc.*), proximal probes, optical components, catalyst supports, and adsorbents.[8−11] However, a number of approaches have been reported in the literature for the fabrication of carbon films including chemical vapor deposition, ultrasonic deposition, pyrolysis of polymer

* Address correspondence to mukeshiitd@gmail.com, ionov@ipfdd.de.

Received for review March 5, 2015 and accepted May 26, 2015.

Published online May 26, 2015
10.1021/acsnano.5b01406

coatings, and hydrothermal decomposition of carbide compounds, but fabrication of mesoporous carbon materials with an ordered structure has been a challenge for material scientists. One of the most commonly employed protocols for fabrication of such materials exploits hard templates to create ordered replicas.[12,13] Since Ryoo *et al*. first reported the synthesis of mesoporous carbon materials (CMK-1,4) via a nanocasting route using mesoporous silica MCM-48 as a hard template,[7] various types of mesoporous silica and carbon precursors have been adapted to synthesize mesoporous carbons, such as CMK-2 from SBA-1[14,15] and CMK-3 and CMK-5 from SBA-15.[16,17]

In recent years, structure-guiding templates derived from self-assembled block copolymers have been identified as a promising tool for fabrication of well-defined material architectures. The self-assembly of two dissimilar covalently bound polymer chains leads to the formation of a variety of polymer templates with fascinating morphologies possessing periodicities on the 10 nm length scale.[18] By careful manipulation of the total block length, the composition of the blocks, and the strength of the interaction between the blocks of copolymers the morphology can be as varied as lamellae (1D), hexagonally packed cylinders (2D), body-centered cubic spheres (3D), or bicontinuous gyroids (3D).[19] A variety of metal/metal oxide nanodots and nanowires have been fabricated by exploiting cylindrical and lamella morphologies of self-assembled block copolymers, respectively.[20−23] Such nanostructures usually exhibit only in-plane continuity in thin films, but for most of the above-mentioned applications of the porous carbon materials, especially in energy storage/conversion devices, three-dimensional interconnected networks with uniform porosity are critical to the performance. In order to fabricate such nanostructures, nanotemplates derived from bicontinuous double-gyroid morphology of the self-assembled block copolymers have been found most appealing as structure-guiding templates. In this fascinating morphology, two interwoven continuous networks of the minority polymer block are held in a matrix phase of the majority block, which is centered on a gyroid surface.[13,24−26] The selective degradation of the minor phase by one or another means results in the fabrication of nanotemplates exhibiting fully interconnected channels and struts with uniform porosity and high surface area. Recently, some studies have been reported in the literature on the application of such nanostructures as sacrificial templates to fabricate metal/metal oxide gyroid replicas. For example, Crossland *et al*.[27] reported the fabrication of a free-standing bicontinuous double-gyroid titania network for solar cell applications by exploiting poly(4-fluorostyrene)-*b*-poly(D,L-lactide) (PFS-*b*-PLA) as a template. In another study, Wiesner *et al*.[28] described the preparation of silica-based bicontinuous nanostructures using poly(isoprene-*b*-ethylene oxide) (PI-*b*-PEO) block copolymers with gyroid morphology as a structure-guiding agent. Thomas *et al*.[14] have demonstrated the preparation of gyroid silica networks with an extremely low refractive index (1.1) by employing polystyrene-*b*-poly(L-lactide) (PS−PLLA) as a sacrificial template. In another set of studies, Steiner *et al*.[29] employed the double-gyroid morphology of a polystyrene-*b*-polyisoprene (PS-*b*-PI) block copolymer to achieve calcite single crystals, while Chen *et al*.[30] used polybutadiene-*b*-poly(dimethylsiloxane) (PB-*b*-PDMS) block copolymer templates to fabricate conducting gyroid-polypyrrole networks. Loos *et al*. demonstrated the use of gyroid morphology for the fabrication of metallic foams.[31] Recently Wiesner *et al*. also reported the fabrication of porous carbon material using block copolymers with gyroid structure.[32]

In this study, we explore the fabrication and characterization of such novel carbon materials by employing polystyrene-*b*-poly(4-vinylpyridine) (PS-*b*-P4VP) block copolymers and the amphiphilic molecule 3-pentadecylphenol (PDP), which together form a gyroid morphology as a sacrificial template. We apply the obtained nanoporous carbon as a material to design cathodes for lithium sulfur batteries, which have a very high theoretic specific energy of 2600 Wh/kg due to the extraordinary theoretical specific capacity of 1675 mAh/g of sulfur.

RESULTS AND DISCUSSION

In this paper we used block copolymers, which form a gyroid morphology, to fabricate porous carbon cathodes for lithium sulfur batteries. As schematically shown in Figure 1, first, nanoporous templates with gyroid morphology are fabricated by selective removal of pentadecylphenol molecules from the PS-(P4VP-PDP) supramolecular complex (Figure 1a,b). The formed nanoporous templates are filled with carbon precursor solution, *i.e*., resorcinol−formaldehyde resin (Figure 1c), cross-linked, and finally carbonized at elevated temperature in inert media to fabricate the gyroid carbon replicas (Figure 1d) with uniform porosity and high surface area. The formed nanoporous carbon is then filled with sulfur and used as a material for the cathodes (Figure 1e).

The Flory−Huggins interaction parameter between polystyrene (PS) and poly(4-vinylpyridine) (P4VP) (χ = 0.35)[33,34] indicates that a PS-*b*-P4VP diblock copolymer will be in the strong segregation limit except for small molar masses and thus limit the possibility of a bicontinuous gyroid self-assembly.[26] However, the addition of a small amphiphilic molecule such as 3-pentadecylphenol has been found to reduce the effective interaction parameter between the two phases and allows the system to self-assemble in a gyroid morphology (Figure 2a).[31] PS-*b*-P4VP diblock copolymer and the amphiphilic agent PDP were dissolved in chloroform

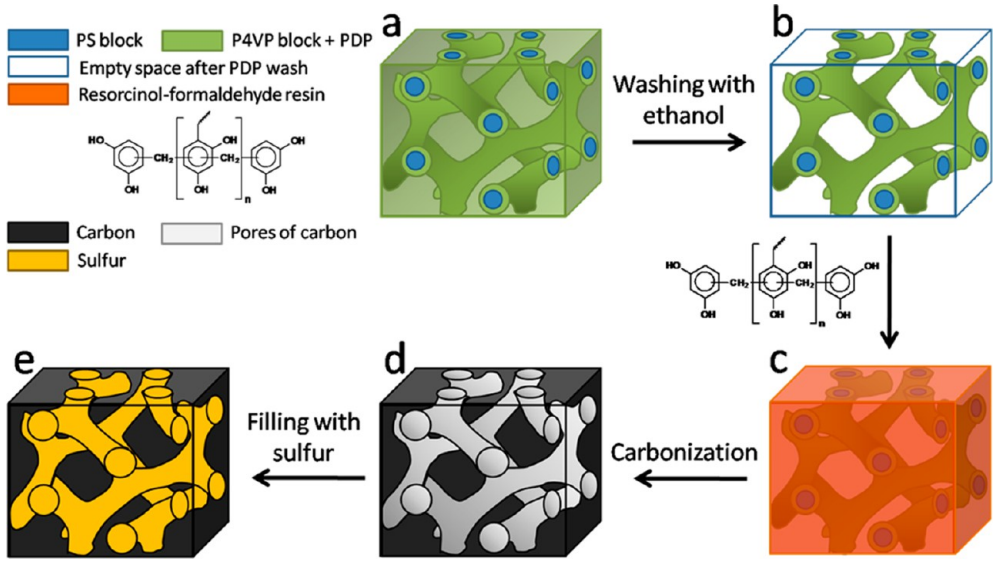

Figure 1. Schematic illustration of the employed approach for the fabrication of gyroid carbon replicas.

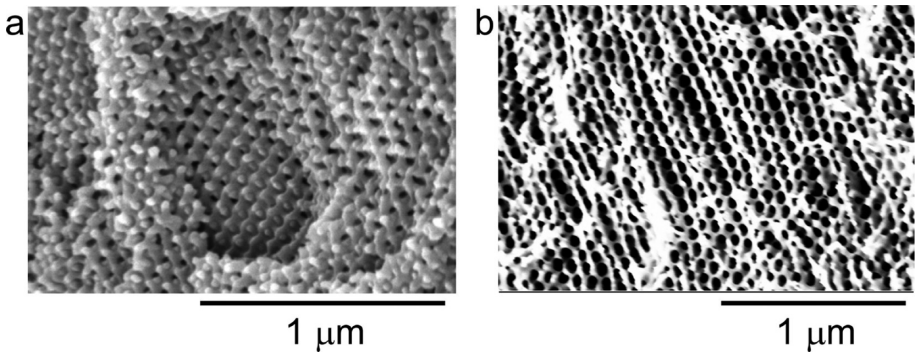

Figure 2. SEM images of PS-P4VP(PDP) complexes before (a) and after (b) removal of PDP.

and annealed in an atmosphere saturated with chloroform to make the PS-(P4VP-PDP) supramolecular complex. Owing to the hydrogen-bonding interaction between the hydroxyl groups and nitrogen atoms of the pyridine rings, PDP prefers to assemble into the P4VP phase. After annealing for several days, chloroform was allowed to evaporate, and white-colored free-standing block copolymer films were obtained. A selective washing of PDP molecules from the block copolymer films in ethanol resulted in the formation of a nanoporous template with gyroid morphology exhibiting PS struts coated with P4VP chains (Figure 2b). In order to investigate the morphology, samples have been analyzed with electron microscopy. Figure 2a and b show representative SEM images of PS-*b*-(P4VP-PDP) complexes before and after ethanol washing, respectively. These images prove the fabrication of a highly porous polymer film exhibiting almost uniformly distributed and interconnected pores after selective removal of the PDP from the PS-(P4VP-PDP) complex.

To confirm the removal of PDP from the PS-*b*-(P4VP-PDP) complex, samples have been studied by FTIR spectroscopy. Figure 3 shows the FTIR spectra of the PS-*b*-(P4VP-PDP) complex before and after the ethanol wash. One can observe a significant decrease in intensity of the C−O stretching vibrations of the PDP molecules at 1145 and 1230 cm^{-1}. In addition, the intensity of the C═C aromatic stretching vibrations at 1600 cm^{-1} has also been observed to decrease after the ethanol treatment, indicating loss of aromatic content from the sample, attributable to the removal of PDP from the complex. It is noteworthy that PDP-characteristic bands have not disappeared completely in the ethanol-treated sample, which suggests the presence of a small amount of PDP in the nanoporous template.

Resorcinol−formaldehyde resin is known as a promising carbon precursor material due to the high aromatic content, and it has been frequently used for the fabrication of porous carbon materials by impregnating into templates followed by pyrolyzing in an inert media.[35] We also use this resin as a precursor and impregnated into fabricated porous gyroid templates. To ensure the complete filling of the available porous area in the template, air has been sucked out from the pores by applying a vacuum before impregnation with

resin solution. Moreover, the hydrophilic nature rendered by the P4VP phase of the channel walls of these porous structures facilitates the impregnation of aqueous resin solution deep inside the templates. As visualized in the microscopic analysis (Figure 4a–d), template films have nanoscaled interconnected channels; therefore capillary forces can also be expected to facilitate the penetration of the solution inside the film. Most importantly, the presence of the polar P4VP corona around the PS struts in the gyroid templates formed after selective removal of the PDP molecules from the PS-(P4VP-PDP) complex promotes the wetting

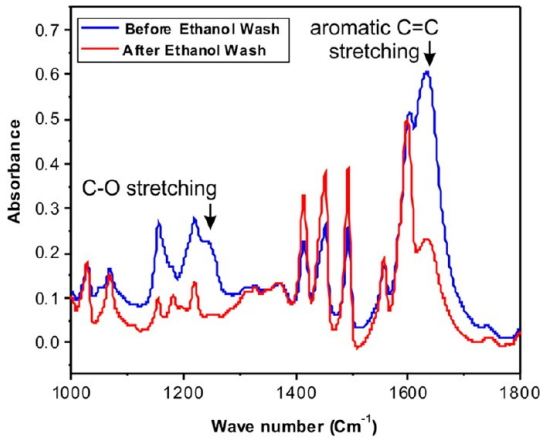

Figure 3. FTIR spectra of the PS-P4VP(PDP) complex before and after the ethanol wash.

of pores with the aqueous solution of resorcinol–formaldehyde. After impregnation with resin solution, white-colored porous nanotemplate films have been found to turn yellowish-brown, indicating the filling of the pores.

In a subsequent step, samples were heated at 80 °C for 4 days, resulting in the formation of cross-linked resorcinol–-formaldehyde resin inside the gyroid templates. Finally, resin-filled samples were pyrolyzed at elevated temperature in an inert media to get highly porous gyroid carbon replicas. Pyrolysis of the samples not only converts the cross-linked resin into carbon but also removes the PS phase, leaving behind an interconnected porous carbon network with a high surface area. Figure 4a shows a representative SEM image of gyroid carbon replicas obtained after pyrolysis of resin-filled gyroid nanotemplates, revealing a highly ordered and porous structure across the bulk sample. Figure 4b shows a magnified top view of the same sample, indicating interconnected channels of fabricated porous carbon material.

TEM analysis has also been employed to study the morphology of fabricated carbon nanostructures. Figure 4c,d reveal representative TEM images of a gyroid carbon replica at different magnifications. One can clearly observe a highly ordered and uniform porous structure of gyroid carbon replicas. The dark-colored areas represent the walls of the carbon network, while free space appears light gray in these

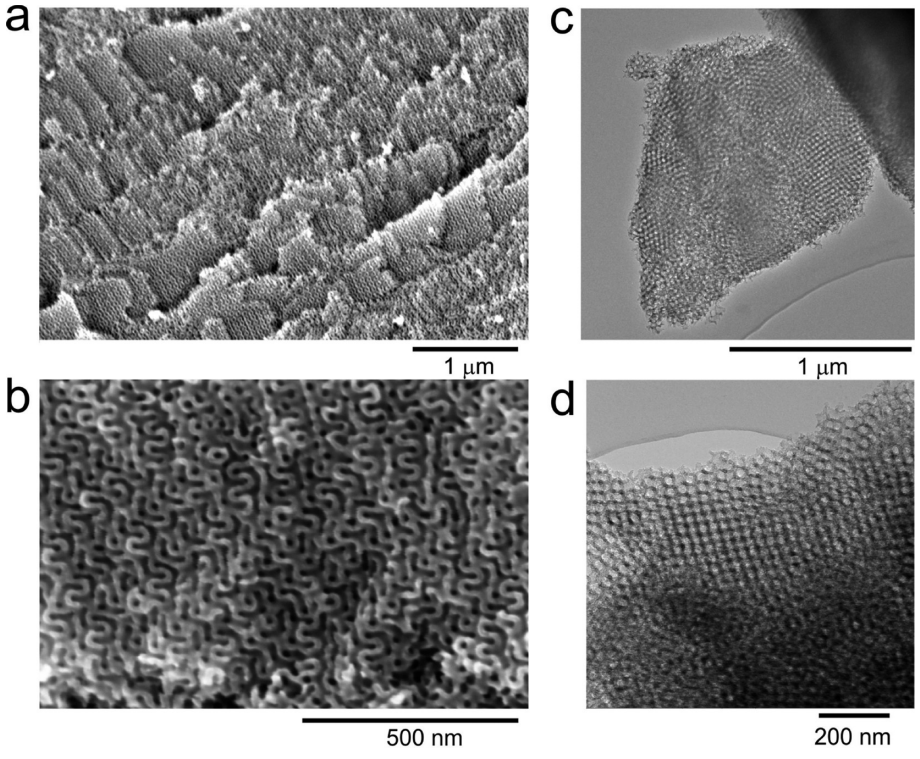

Figure 4. Structure of nanoporous carbon obtained using block copolymers. (a) Overview and (b) magnified SEM images of carbon nanostructures, obtained after calcination of resorcinol–formaldehyde-filled gyroid nanotemplates. (c, d) TEM images of highly porous gyroid carbon replicas at different magnifications.

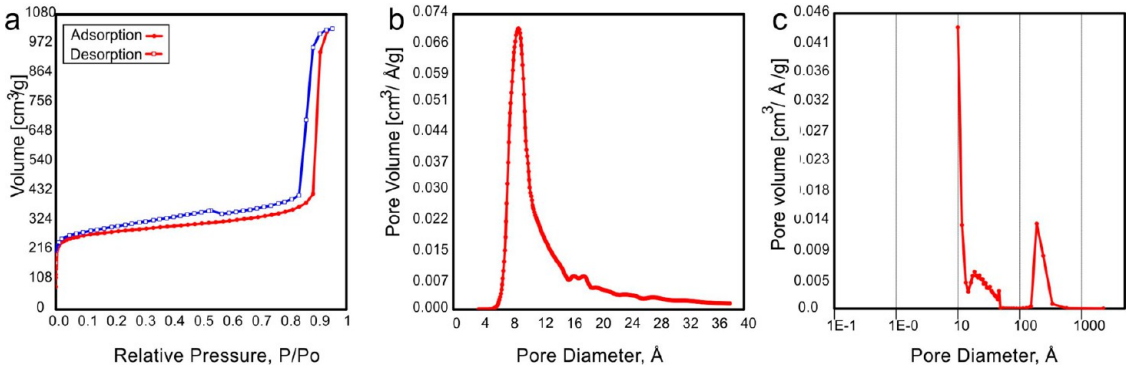

Figure 5. Nitrogen adsorption−desorption isotherms at 77 K: (a) micro- and (b) mesopore size distribution for nanoporous carbon.

images of the porous carbon material. These results suggest that the carbon replica remains stable after the thermal treatment and retains the inverse gyroid morphology imposed by the structure of the porous polymer template.

It is noteworthy to mention here that mixing of the PDP molecule in the diblock copolymer helped in fabricating the carbon material with a high porosity and surface area because the PS(core)-P4VP(corona) gyroid network occupies more than 50 vol % in such complexes. In contrast, a conventional bicontinuous gyroid diblock copolymer structure would result in a highly porous template (porosity *ca.* 65 vol %) after the selective removal of the matrix-forming block and thus a correspondingly far less porous (*ca.* 35 vol %) carbon nanostructure. Additionally, removal of the chemically degradable matrix such as PLA or PEO from the bicontinuous gyroid morphology of their diblock copolymers with PS[36] would result in a porous template exhibiting the hydrophobic surface of the PS struts. For such templates, an extra step of the surface modification of these PS struts would be required for facilitating the penetration of the resin precursor solution.[37] The supramolecular approach described here avoids this issue by the presence of the hydrophilic P4VP corona on PS struts, which promotes the penetration of the water-based carbon precursor into the porous template.

To confirm the porous nature of the fabricated carbon material, surface area and porosity measurements have been carried out using a nitrogen adsorption/desorption method. Figure 5a reveals that the fabricated sample follows a typical IV type physisorption isotherm. An increase in nitrogen uptake at high relative pressure $P/P_0 = 0.9-1.0$ and a wide hysteresis loop suggest that the fabricated sample is mesoporous in nature. Following the Brunauer−Emmett−Teller (BET) method, the specific surface area has been estimated as 885 $m^2\ g^{-1}$, which is comparable to that reported in the literature.[32] As shown in Figure 5b and c, the sample has been found to have pores with sizes in both the micro and meso ranges. The SF (Saito−Foley) and BJH (Barrett−Joyner−Halenda) methods have been employed to estimate the pore sizes in the micro (<2 nm) and meso ranges (2−50 nm), respectively. A meager distribution of mesopores with a pore diameter around 20 nm and micropores with a pore diameter around 1 nm has been observed. It is speculated that mesopores are formed by the degradation of the polymer template, while micropores are generated by the volatile components evolved during the pyrolysis of the resorcinol−formaldehyde resin filled polymer templates. On the other hand, the porous carbon derived by carbonization of the resorcinol−formaldehyde resin without a polymer template consists only of micropores and has a far lower value of BET surface area of 280 m^2/g (see Figure S1 in the Supporting Information). The effect of having the three-dimensionally ordered structure with bimodal porosity of gyroid templated carbon is expected to reflect the electrochemical performance of the carbon−sulfur cathode.

The nanostructured carbon materials, prepared from a gyroid-templating approach, have been used as a housing for elemental sulfur to prepare the cathode for Li−sulfur batteries. In such electrodes, conductivity of the carbon material is critical to the performance. The carbon material derived from our approach has been found to possess an electrical conductivity of 365 mS/cm, which is lower than that reported by Wiesner *et al.*,[32] which can be caused by fine grinding. This conductivity should, however, be sufficient to realize a good performance of the resulting carbon−sulfur composites as a cathode in Li−S batteries that is sufficient for maintaining electrical contact between carbon and sulfur.

Raman spectroscopy is a powerful analytical tools for characterizing carbon materials. The Raman spectrum of fabricated gyroid carbon replicas is shown in Figure 6a. As expected, one can observe two strong peaks centered at 1345 and 1598 cm^{-1}, which can be assigned as first-order D and G bands of the carbon material, respectively. Another broad peak at 2720 cm^{-1} can be attributed to the second-order D

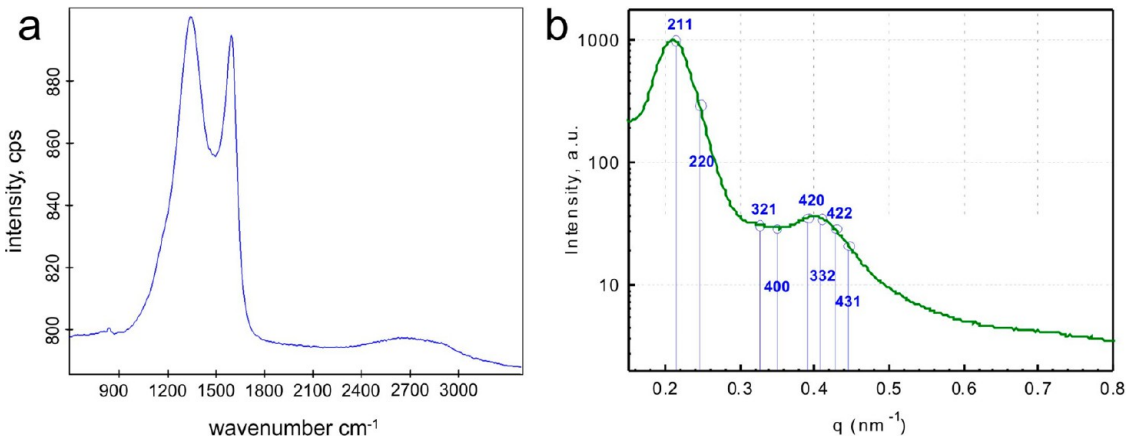

Figure 6. Raman spectra and small-angle X-ray scattering (SAXS) intensity profile with respect to the allowed reflecting lattice planes (blue numbers: *hkl*) of the assumed gyroid carbon structure (reflection intensities are adapted by lines to the scattering profile).

band. It is known from the literature that the D band is related to the C−C stretching vibrations of the disordered sp^3 carbon structure, while the G band corresponds to the C−C stretching vibrations of the planar sp^2 carbon structure as in conventional graphite structures.[38] The D/G intensity ratio of these bands was calculated considering the complete peak areas under the D and G band and was found to be 1.63. The D/G intensity ratio signifies the degree of order (content of graphitization) in the carbon material. In pristine graphite materials the D/G ratio is usually very small. If the D/G ratio is higher, like in this material, then the degree of defects in the planar carbon graphite structure is relatively high.[39] So, these results suggest that the fabricated sample is a mixture of disordered and ordered (graphitized) carbon structures with a relatively high content of disordered sp^3 carbon structures, like in amorphous carbon.

In order to further investigate the structural aspects of fabricated porous carbon material, samples have been characterized by small-angle X- ray scattering, and the results are shown in Figure 6b. One can observe the scattering pattern with a mutual gyroid structure having a cubic unit cell parameter a = 72.0 nm (Figure 6b). The first eight possible reflections (*i.e.*, the allowed ones assigned by Miller indices (*hkl*) beginning with (211)) in this model are arranged with the following q-ratios, which fits with the structure of nanoporous carbon prepared from gyroid templating.

In the subsequent step, elemental sulfur was diffused into the fabricated porous carbon structures to prepare carbon−sulfur composites. For this purpose, sulfur was physically mixed with porous carbon in a ball mill, and then the resulting mixture was heat treated at 155 °C for 5 h (Figure 7a). As elemental sulfur is known to show the lowest viscosity at 155 °C, this temperature has been chosen to heat treat the premixed carbon−sulfur composites.[40] This heat treatment helps in filling the majority of the channels of the porous carbon material with sulfur by capillary forces. Moreover, the hydrophobic nature of highly porous carbon material facilitates the infiltration of molten sulfur. Figure 7a shows the SEM image of a physically mixed and heat-treated carbon−sulfur mixture. One can observe sulfur clusters adhered onto the surface of the porous carbon structures. At the end a carbon−sulfur composite with uniformly distributed sulfur was achieved, and the homogeneity is observed from the SEM images (Figure 7b). The homogeneous distribution of sulfur in the porous carbon network was further confirmed by energy-dispersive X-ray spectroscopy (EDX) (Figure 7c).

Finally, we assembled a lithium−sulfur battery using prepared sulfur-infiltrated porous carbon as cathode. The electrochemical properties of porous carbon−sulfur cathodes have been tested by means of cyclovoltammetric and charge/discharge measurements (Figure 8). As shown in Figure 8a, cyclovoltammetric measurements have been performed by charging and discharging the cells between 1 and 3 V. During the discharge cycle, two reduction peaks, at 2.4 and 2 V, were observed. These peaks correspond to the reduction of sulfur to Li_2S_n ($n > 4$) and the subsequent reduction of higher order polysulfides to short-chain polysulfide species, respectively. The charging curve of the battery has been found to show a single peak at 2.4 V. The relatively narrow peaks indicate good reaction kinetics for reduction as well as the oxidation reactions. The plateaus in the voltage profiles (Figure 8b) match with the peak voltages of the cyclic voltammograms for the reduction and oxidation cycles (Figure 8a).

Figure 8c−f show the galvanostatic charge/discharge curves of fabricated Li−S batteries (calculated based on per gram sulfur) cycled within different voltage ranges using electrolytes with and without $LiNO_3$. For all charge−discharge experiments, the cells were charged at double the C-rate compared to the discharge C-rate to simulate a realistic situation where

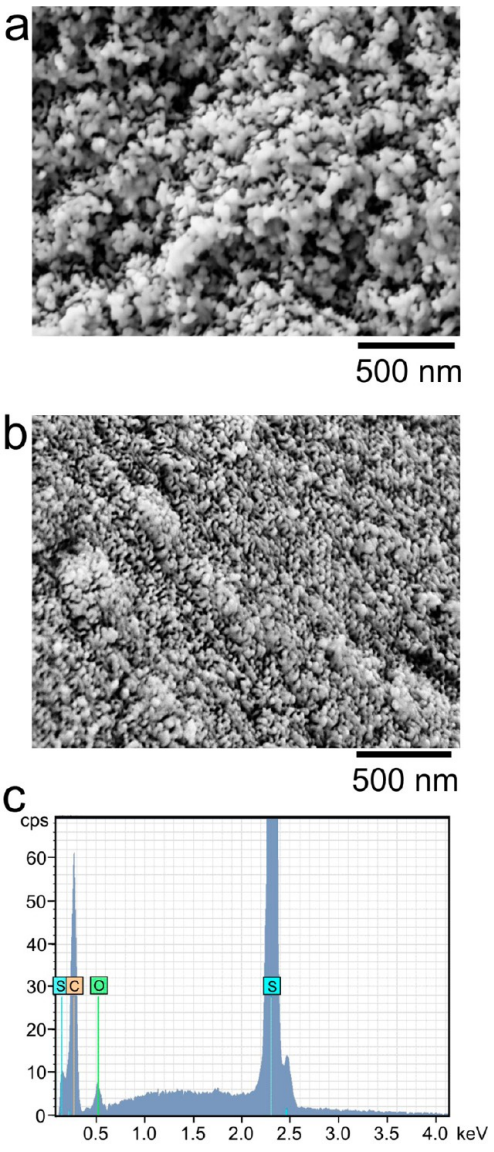

Figure 7. SEM images of a carbon−sulfur composite (a) before thermal annealing and (b) after thermal annealing. (c) EDX spectra of elements of the annealed carbon−sulfur composite.

a faster charging is normally adopted. For these experiments, fabricated cells have been cycled in order to avoid complete charge and discharge of the battery; that is, the voltage range was set to 1.5−2.8 or 1.8−2.6 V. Charging and discharging capacities have been observed in the range of 600 (cycling range 1.8−2.6 V) to 800 mAh/g_{sulfur} (cycling range 1.5−2.8 V). Clearly, the wider the potential window is, the larger the capacity. The Coulombic efficiency was found to be around 80% (without $LiNO_3$) or 100% (with $LiNO_3$), which is known to improve the Coulombic efficiency by creating a protective film comprising Li_xNO_y formed on the Li anode by the reactions of the additive directly with the anode surface.[41] Moreover, it is noteworthy that both charging and discharging capacities have been found to be stable over more than 200 cycles. Interestingly, the cycling experiments performed between 1 and 3 V, which resulted in full discharge and charge of the cell, have been found to show a very fast decay in discharging capacity of the cells from 600 mAh/g_{sulfur} to *ca.* 200 mAh/g_{sulfur} over the first 50 cycles only (see Figure S2 in the Supporting Information). This difference in performance of fabricated Li−S batteries can be attributed to the electrochemical reactions undergone by sulfur between two different voltage windows. Complete charging of the cell results in the formation of insoluble sulfur particles on the cathode, which might lose contact with the electrode during the discharge cycle and may result in a decrease in the effective mass of sulfur participating in the electrochemical reaction. Moreover, full discharging leads to formation of lithium sulfide, which is also insoluble and can be partially excluded from the electrochemical reaction when lithium sulfide particles lose contact with the electrode. On the other hand, incomplete charge and discharge leaves sulfur in the form of polysulfides with different lengths. These polysulfides are soluble in electrolyte and, thus, are available for electrochemical reaction. The soluble higher order lithium polysulfides were used to react with metallic lithium, forming an insulating passivation layer of Li_2S. This effect was restricted by the use of $LiNO_3$ as additive, and improved Coulombic efficiency was achieved (Figure 8e,f). In the experiments with $LiNO_3$ the surface passivation layer of Li_xNO_y does not expose the elemental lithium to the soluble polysulfides; thus it reduces the shuttle effect, which basically prevents the active mass loss by the so-called "shuttle effect", and the capacity loss due to this effect is also compensated. We also investigated the rate capability of batteries assembled using nanoporous cathodes by changing the charging rate from 0.2C to 2C and back to 0.2C (the discharging rate was changed from 0.1C to 1C and back to 0.1C, Figure 8d). We observed that the initial discharge capacity was in the range of 700 mAh/g_{sulfur} at a 0.1C discharge rate. The discharge capacity decreased to *ca.* 400 mAh/g_{sulfur} at a 1C discharge rate and increased back to 700 mAh/g_{sulfur} at a 0.1C discharge rate, which indicates a good electrochemical stability. The obtained values for charging and discharging capacity are comparable to the values reported in the literature, which are around 800−1000 mAh/g_{sulfur}.[42−50] In fact, the direct comparison of different values of capacity is difficult because the measurements are done at different conditions and the performance of the battery is a combination of many factors.

The ordered gyroid-structured carbon material to host sulfur in its high surface area is beneficial with respect to electrochemical performance because of the bimodal porosity generated by decomposition of the polymer template, creating mesopores (pore diameter 2−50 nm), and the evolution of gaseous product

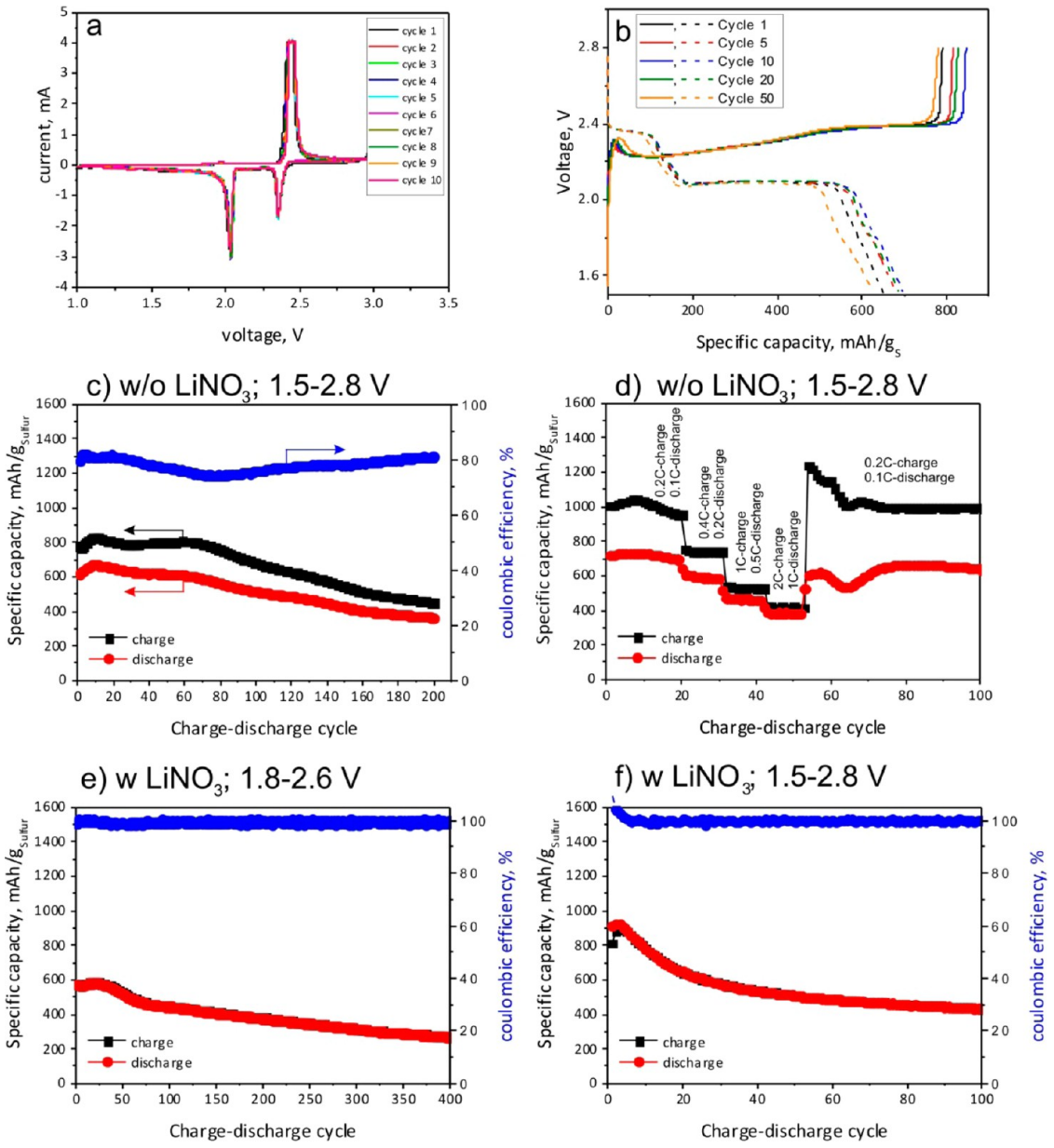

Figure 8. Cyclovoltammetric (a) and voltage profile of the constant-current measurements (b) and charge/discharge measurements (c–f) of Li–S batteries assembled using cathodes with carbon materials obtained from porous carbon with a gyroid structure measured at different conditions (voltage range and presence of $LiNO_3$).

due to the pyrolysis of resorcinol–formaldehyde resin responsible for generating micropores (pore diameter <2 nm). The bimodal porous structure is advantageous for higher active material loading as well as trapping the polysulfides in the narrow micropores. This bimodal porosity gives rise to a high surface area, whereas the carbonized resorcinol–formaldehyde resin without a template has a far lower surface area (~280 m^2/g), charging/discharging capacity, and Coulombic efficiency (see Figure S3 in the Supporting Information), and it is devoid of any ordered structure, which might keep the cell capacity high. The three-dimensionally ordered mesopores demonstrate uniform accessibility of sulfur by the diffused lithium ion throughout the structure and offers structural integrity of the cathode structure with prolonged cycling.

Finally, we compared the obtained capacity with theoretical values. The theoretical capacity of the sulfur electrode is 1.6×10^{-19}(C) $\times$ 6×10^{23} (/mol) $\times$ 2/(32 (g/mol) $\times$ 3600s/h) = 1.67 Ah/g_{sulfur}. This value corresponds to the whole route of conversion from S_8^0 to S^{2-} (Figure 9). In experiments we avoided complete charge and complete discharge, which lead to formation of insoluble S_8^0, S_2^{2-}, and S^{2-}. The energetic capacity of sulfur involved in the reaction $3S_8^{2-} \rightarrow 8S_3^{2-}$, where electrolyte-soluble polysulfides are formed, is 1.6×10^{-19} (C) $\times$ 6×10^{23} (/mol) $\times$ 10/(768 (g/mol) $\times$ 3600s/h) = 0.35 Ah/g_{sulfur}. Our

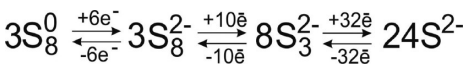

Figure 9. Scheme of the electrochemical conversion of sulfur in Li–S batteries.

batteries demonstrate an intermediate capacity, which is around 0.8 Ah/g_{sulfur}. Thus, we can argue that cycling between 1.6 and 2.8 V leads to formation of some amount of insoluble S_8^0, S_2^{2-}, and S^{2-}.

CONCLUSION

A novel approach to the fabrication of nonporous carbon cathodes with high surface area and uniform porosity for lithium–sulfur batteries has been reported. Self-assembled block copolymer templates with gyroid morphology have been exploited as a structure-directing agent and filled with resorcinol–formaldehyde resin as carbon precursor. Cross-linking and subsequent carbonization of the resin-filled gyroid nanotemplates resulted in the fabrication of gyroid carbon replicas. We applied the prepared porous carbon as a cathode for lithium–sulfur batteries, which demonstrate high charging/discharging capacity, very good rate capability, and high cycling stability for more than 200 cycles. Underlining the unique morphology, fabricated carbon nanostructures with sulfur have been found to have great potential in lithium sulfur batteries by giving uniform accessibility of sulfur by lithium ions in its three-dimensional network structure and demonstrating improved battery performance.

METHODS

Materials. Polystyrene-*b*-poly(4-vinylpyridine) block copolymer (M_n(PS) = 37 500 g/mol, M_n(P4VP) = 16 000 g/mol, M_w/M_n = 1.3) was obtained from Polymer Source Inc. and used as received. Resorcinol, formaldehyde (as 37 wt % formalin solution), and sodium carbonate were purchased from Aldrich and used as received. 3-Pentadecylphenol was also acquired from Aldrich (98% purity) and recrystallized from petroleum ether before use. The lithium-ion battery grade conductive carbon black was provided by Timcal Graphite and Carbon. Elemental sulfur (S_8), polyvinylidine fluoride (PVDF), *N*-methyl-2-pyrrolidone, bis(trifluoromethane)sulfonimide lithium salt (LiTFSI), 1,2-dimethoxyethane (DME), 1,3-dioxolane (DOL), and lithium nitrate (>99% purity) were purchased from Sigma-Aldrich, Germany, and used without further purification. Nickel foil of thickness 20 μm was procured from Schlenk Metallfolien GmbH. Electrochemical-grade high-purity (99.9%) lithium was purchased from LinYiGelon New Battery Materials Co. Ltd., China. Porous polypropylene membrane was used as separator.

Preparation of Nanoporous Gyroid Templates. PS-*b*-P4VP block copolymer and PDP ($PDP_{mol}/P4VP_{mol}$ = 0.8) were dissolved in chloroform at 1.5 wt % concentration, and the resulting solution was stirred for 2 h at room temperature. The filtered solution was poured into a glass bottle and annealed in a saturated chloroform atmosphere for 11 days. Next, chloroform was allowed to evaporate slowly, and the resulting casted films were heat treated at 130 °C for 20 min. Afterward, films were peeled off from the glass vessel and stirred in ethanol for 3 days at room temperature to remove PDP molecules from the PS-(P4VP-PDP) complex, resulting in the formation of PS-P4VP gyroid nanoporous templates.

Fabrication of Gyroid Carbon Replicas. The nanoporous polymer films were treated with oxygen plasma on both sides and then subjected to vacuum for 3 h to reduce the air pressure inside the pores, so that the resin precursor solution can penetrate into the porous template. The resorcinol–formaldehyde solution was prepared by dissolving resorcinol in formaldehyde (37 wt % formalin solution) in 1:1.8 molar ratios and adding a small amount of Na_2CO_3 as catalyst (1:0.017 molar ratio of resorcinol to Na_2CO_3) dissolved in water at 10 wt % concentration. This resin precursor solution was allowed to fill the nanoporous template for 2 h, which turned the white-colored porous polymer film to yellowish-brown. Samples were heated in a closed vessel for 4 days and then for 1 day in an open vessel at 80 °C to cross-link the resorcinol–formaldehyde resin. Finally, the resulting dark red colored films were carbonized at 900 °C at 5 K/min for 2 h in an argon atmosphere to obtain the gyroid carbon replicas.

Fabrication of Gyroid Carbon–Sulfur Composite Cathode. As-prepared gyroid-structured carbon was mixed with elemental sulfur in a ball mill by keeping the weight ratio of carbon to sulfur as 1:2. The carbon–sulfur composite powder was heated at 155 °C to facilitate the infiltration of very low viscous sulfur melt. It was allowed to anneal at 155 °C for 5 h to ensure complete filling of the carbon pores by sulfur and followed by heat treatment at 300 °C for 2 h to remove excess sulfur adhered onto the surface. In the next step, the cathode was prepared by mixing the carbon– sulfur composite material (82 wt %), PVDF binder (8 wt %), and carbon black (10 wt %) as conducting additive in *N*-methyl-2-pyrrolidone. The slurry was then coated on nickel foil acting as a current collector followed by drying at 60 °C for 12 h under vacuum.

Analytical Characterization. Scanning electron microscopy (SEM) images were recorded on a NEON40 microscope (Carl Zeiss Microscopy GmbH, Oberkochen, Germany) at an accelerating voltage of 3 kV. Specimens were prepared by fixing small pieces of the samples on a stub with conducting tape and coating them with a 3 nm layer of platinum.

Transmission electron microscopy (TEM) analysis was carried out in a Libra 200 microscope (Carl Zeiss Microscopy GmbH, Oberkochen, Germany) at 200 keV. The specimens were prepared by grinding a small grain of carbon sample and dispersing it into the ethanol followed by placing a drop on a TEM grid. Samples were dried at 50 °C to remove all traces of ethanol before TEM investigation.

X-ray scattering analysis was done on an XRD 3003 θ/θ diffractometer (GE Inspection Technologies, Ahrensburg, Germany) by irradiating the powdery samples, mounted in a glass tube of 1 mm diameter and 0.01 mm wall thickness, with a Cu Kα monochromatic beam (1.54 Å). The carbon powder sample in a glass capillary was used for the measurement of small-angle X-ray scattering (SAXS) in the range of 0.2° to 5°.

Raman spectra were taken on a WITEC alpha 300R Raman Imaging System by irradiating the samples with laser light having a 1 mW power and 532 nm wavelength. FTIR spectra were recorded on a Vertex 80 V FTIR spectrometer (Bruker). Prior to analysis, dried samples were mixed with KBr and pressed into a tablet. Surface area and porosity measurements were carried out on an Autosorb-1 instrument from Quantachrome, USA, at 77.4 K by using nitrogen as adsorbent. Prior to analysis, samples were dried at 80 °C for 2 h.

Conductivity of the powder sample was measured in an in-house-built device with custom-made software. The carbon sample was ground to a powdery form in a ball mill prior to measurement. The powder to be examined was filled into a hollow PMMA cylinder and compressed by a piston. During the compression process, the electric resistance was continuously measured between two electrodes situated on top of the piston and on the bottom of the cylinder by DMM 2001 Keithley Instruments. The conductivity derived from the resistance and the geometry data was then recorded against the pressure. The control of the device as well as the data acquisition and analysis

was carried out by custom-made software developed with TestPoint. The software allows user programming of different cycles and automatic control. The pressure between the electrodes was maintained up to a maximum value of 1 MPa to avoid rupturing of the carbon nanostructures.

Energy-dispersive X-rays were obtained in an Ultra Plus (Carl Zeiss Microscopy GmbH, Oberkochen Germany) scanning electron microscope and a Quantax EDX detector (Bruker AXS GmbH, Berlin, Germany). A primary beam of 20 keV was used for these measurements. The carbon–sulfur composite powder samples were adhered on a double-sided adhesive carbon and coated with carbon using carbon filament vapor deposition to reduce charging at high magnification.

Electrochemical Characterization. Electrochemical measurements were done by means of cyclic voltammetry and constant current measurements. The coin-type cathodes were cut as discs from the entire piece, and 2032 coin cells were assembled in an argon-filled glovebox, keeping the carbon–sulfur composite electrode as the cathode, lithium metal discs as the anode, and the porous polypropylene membrane as the separator. Electrolytes with two different compositions were made: one containing 1 M LiTFSI in 1:1 (v/v) DME and DOL and another containing 0.25 M lithium nitrate and 1 M LiTFSI in 1:1 (v/v) DME and DOL. The separators were soaked with 100 μL of the respective electrolyte during cell assembly. Cyclic voltammetry was performed in an Ivium-nStatpotentiostat-galvanostat within the potential range of 1 to 3 V at a scan rate of 100 μV/s. Galvanostactic charge/discharge tests were carried out in a BST8-MA 8 channel battery analyzer at a constant current density of 336 mA/g (0.2 C) for charging and 168 mA/g (0.1 C) for discharging within the potential window of 1.5 to 2.8 V.

Conflict of Interest: The authors declare no competing financial interest.

Supporting Information Available: The BET result and charge–discharge measurement of carbon derived from resorcinol–formaldehyde resin without gyroid template. The Supporting Information is available free of charge on the ACS Publications website at DOI: 10.1021/acsnano.5b01406.

Acknowledgment. The authors greatly acknowledge German Research Foundation (DFG) SPP 1473 and German Ministry for Research and Education (BMBF) BaMoSa-03X4637A-H for financial support.

Note Added after ASAP Publication: This paper posted ASAP on May 29, 2015. The Supporting Information file was corrected and the revised version was reposted on June 4, 2015.

REFERENCES AND NOTES

1. Corma, A. From Microporous to Mesoporous Molecular Sieve Materials and Their Use in Catalysis. *Chem. Rev.* **1997**, *97*, 2373–2420.
2. Davis, M. E. Ordered Porous Materials for Emerging Applications. *Nature* **2002**, *417*, 813–821.
3. Li, L.; Shi, J.-l.; Yan, J.-n. A Highly Efficient Heterogeneous Catalytic System for Heck Reactions with a Palladium Colloid Layer Reduced *in Situ* in the Channel of Mesoporous Silica Materials. *Chem. Commun.* **2004**, 1990–1991.
4. Shi, J.-l.; Hua, Z.-l.; Zhang, L.-x. Nanocomposites from Ordered Mesoporous Materials. *J. Mater. Chem.* **2004**, *14*, 795–806.
5. Vallet-Regí, M. Ordered Mesoporous Materials in the Context of Drug Delivery Systems and Bone Tissue Engineering. *Chem.—Eur. J.* **2006**, *12*, 5934–5943.
6. Ying, J. Y.; Mehnert, C. P.; Wong, M. S. Synthesis and Applications of Supramolecular-Templated Mesoporous Materials. *Angew. Chem., Int. Ed.* **1999**, *38*, 56–77.
7. Ryoo, R.; Joo, S. H.; Jun, S. Synthesis of Highly Ordered Carbon Molecular Sieves via Template-Mediated Structural Transformation. *J. Phys. Chem. B* **1999**, *103*, 7743–7746.
8. Lee, J.; Yoon, S.; Hyeon, T.; M. Oh, S.; Bum Kim, K. Synthesis of a New Mesoporous Carbon and its Application to Electrochemical Double-Layer Capacitors. *Chem. Commun.* **1999**, 2177–2178.
9. Wen, Z.; Liu, J.; Li, J. Core/Shell Pt/C Nanoparticles Embedded in Mesoporous Carbon as a Methanol-Tolerant Cathode Catalyst in Direct Methanol Fuel Cells. *Adv. Mater.* **2008**, *20*, 743–747.
10. Wang, H.; Wang, A.; Wang, X.; Zhang, T. One-Pot Synthesized MoC Imbedded in Ordered Mesoporous Carbon as a Catalyst for N_2H_4 Decomposition. *Chem. Commun.* **2008**, 2565–2567.
11. Vinu, A.; Miyahara, M.; Mori, T.; Ariga, K. Carbon Nanocage: a Large-Pore Cage-Type Mesoporous Carbon Material as an Adsorbent for Biomolecules. *J. Porous Mater.* **2006**, *13*, 379–383.
12. Lu, A. H.; Schüth, F. Nanocasting: A Versatile Strategy for Creating Nanostructured Porous Materials. *Adv. Mater.* **2006**, *18*, 1793–1805.
13. Agrawal, M.; Choudhury, S.; Gruber, K.; Simon, F.; Fischer, D.; Albrecht, V.; Göbel, M.; Koller, S.; Stamm, M.; Ionov, L. Porous Carbon Materials for Li–S Batteries Based on Resorcinol–Formaldehyde Resin with Inverse Opal Structure. *J. Power Sources* **2014**, *261*, 363–370.
14. Hsueh, H.-Y.; Chen, H.-Y.; She, M.-S.; Chen, C.-K.; Ho, R.-M.; Gwo, S.; Hasegawa, H.; Thomas, E. L. Inorganic Gyroid with Exceptionally Low Refractive Index from Block Copolymer Templating. *Nano Lett.* **2010**, *10*, 4994–5000.
15. Ryoo, R.; Joo, S. H.; Jun, S.; Tsubakiyama, T.; Terasaki, O. Ordered Mesoporous Carbon Molecular Sieves by Templated Synthesis: the Structural Varieties. *Stud. Surf. Sci. Catal.* **2001**, *135*, 150.
16. Jun, S.; Joo, S. H.; Ryoo, R.; Kruk, M.; Jaroniec, M.; Liu, Z.; Ohsuna, T.; Terasaki, O. Synthesis of New, Nanoporous Carbon with Hexagonally Ordered Mesostructure. *J. Am. Chem. Soc.* **2000**, *122*, 10712–10713.
17. Joo, S. H.; Choi, S. J.; Oh, I.; Kwak, J.; Liu, Z.; Terasaki, O.; Ryoo, R. Ordered Nanoporous Arrays of Carbon Supporting High Dispersions of Platinum Nanoparticles. *Nature* **2001**, *412*, 169–172.
18. Toombes, G. E. S.; Finnefrock, A. C.; Tate, M. W.; Ulrich, R.; Wiesner, U.; Gruner, S. M. A Re-evaluation of the Morphology of a Bicontinuous Block Copolymer–Ceramic Material. *Macromolecules* **2007**, *40*, 8974–8982.
19. Bates, F. S.; Fredrickson, G. H. Block copolymers - Designer Soft Materials. *Phys. Today* **1999**, *52*, 32–38.
20. Kuila, B. K.; Rama, M. S.; Stamm, M. Supramolecular Assembly of Poly(styrene)-b-poly(4-vinylpyridine) and Ferroceneacetic Acid: An Easy Way to Large-Scale Controllable Periodic Arrays of Iron Oxide Nanomaterials. *Adv. Mater.* **2011**, *23*, 1797–1800.
21. Chai, J.; Buriak, J. M. Using Cylindrical Domains of Block Copolymers To Self-Assemble and Align Metallic Nanowires. *ACS Nano* **2008**, *2*, 489–501.
22. Aizawa, M.; Buriak, J. M. Block Copolymer Templated Chemistry for the Formation of Metallic Nanoparticle Arrays on Semiconductor Surfaces. *Chem. Mater.* **2007**, *19*, 5090–5101.
23. Nandan, B.; Kuila, B. K.; Stamm, M. Supramolecular Assemblies of Block Copolymers as Templates for Fabrication of Nanomaterials. *Eur. Polym. J.* **2011**, *47*, 584–599.
24. Hajduk, D. A.; Harper, P. E.; Gruner, S. M.; Honeker, C. C.; Kim, G.; Thomas, E. L.; Fetters, L. J. The Gyroid: A New Equilibrium Morphology in Weakly Segregated Diblock Copolymers. *Macromolecules* **1994**, *27*, 4063–4075.
25. Schulz, M. F.; Bates, F. S.; Almdal, K.; Mortensen, K. Epitaxial Relationship for Hexagonal-to-Cubic Phase Transition in a Book Copolymer Mixture. *Phys. Rev. Lett.* **1994**, *73*, 86–89.
26. Matsen, M. W.; Schick, M. Stable and Unstable Phases of a Diblock Copolymer Melt. *Phys. Rev. Lett.* **1994**, *72*, 2660–2663.
27. Crossland, E. J. W.; Kamperman, M.; Nedelcu, M.; Ducati, C.; Wiesner, U.; Smilgies, D. M.; Toombes, G. E. S.; Hillmyer, M. A.; Ludwigs, S.; Steiner, U.; *et al.* Bicontinuous Double Gyroid Hybrid Solar Cell. *Nano Lett.* **2008**, *9*, 2807–2812.

28. Jain, A.; Toombes, G. E. S.; Hall, L. M.; Mahajan, S.; Garcia, C. B. W.; Probst, W.; Gruner, S. M.; Wiesner, U. Direct Access to Bicontinuous Skeletal Inorganic Plumber's Nightmare Networks from Block Copolymers. *Angew. Chem., Int. Ed.* **2005**, *117*, 1252–1255.
29. Finnemore, A. S.; Scherer, M. R. J.; Langford, R.; Mahajan, S.; Ludwigs, S.; Meldrum, F. C.; Steiner, U. Nanostructured Calcite Single Crystals with Gyroid Morphologies. *Adv. Mater.* **2009**, *21*, 3928–3932.
30. Guo, F.; Schulte, L.; Zhang, W.; Vigild, M. E.; Ndoni, S.; Chen, J. Gyroid Nanoporous Scaffold for Conductive Polymers. *Polym. Chem.* **2011**, *2*, 553–555.
31. Vukovic, I.; Punzhin, S.; Vukovic, Z.; Onck, P.; De Hosson, J. T. M.; ten Brinke, G.; Loos, K. Supramolecular Route to Well-Ordered Metal Nanofoams. *ACS Nano* **2011**, *5*, 6339–6348.
32. Werner, J. G.; Hoheisel, T. N.; Wiesner, U. Synthesis and Characterization of Gyroidal Mesoporous Carbons and Carbon Monoliths with Tunable Ultralarge Pore Size. *ACS Nano* **2013**, *8*, 731–743.
33. Alberda van Ekenstein, G. O. R.; Meyboom, R.; ten Brinke, G.; Ikkala, O. Determination of the Flory–Huggins Interaction Parameter of Styrene and 4-Vinylpyridine Using Copolymer Blends of Poly(styrene-co-4-vinylpyridine) and Polystyrene. *Macromolecules* **2000**, *33*, 3752–3756.
34. Zha, W.; Han, C. D.; Lee, D. H.; Han, S. H.; Kim, J. K.; Kang, J. H.; Park, C. Origin of the Difference in Order–Disorder Transition Temperature between Polystyrene-block-poly(2-vinylpyridine) and Polystyrene-block-poly(4-vinylpyridine) Copolymers. *Macromolecules* **2007**, *40*, 2109–2119.
35. Wang, Z.; Li, F.; Ergang, N. S.; Stein, A. Effects of Hierarchical Architecture on Electronic and Mechanical Properties of Nanocast Monolithic Porous Carbons and Carbon–Carbon Nanocomposites. *Chem. Mater.* **2006**, *18*, 5543–5553.
36. Mao, H.; Hillmyer, M. A. Macroscopic Samples of Polystyrene with Ordered Three-Dimensional Nanochannels. *Soft Matter* **2006**, *2*, 57–59.
37. Kobayashi, Y.; Tadaki, Y.; Nagao, D.; Konno, M. Deposition of Gold Nanoparticles on Polystyrene Spheres by Electroless Metal Plating Technique. *J. Phys. Conf. Ser.* **2007**, *61*, 582–586.
38. Dresselhaus, M. S.; Jorio, A.; Hofmann, M.; Dresselhaus, G.; Saito, R. Perspectives on Carbon Nanotubes and Graphene Raman Spectroscopy. *Nano Lett.* **2010**, *10*, 751–758.
39. Hodkiewicz, J. Characterizing Carbon Materials with Raman Spectroscopy; Thermo Fisher Scientific: Madison, WI, **2010**, Application Note 51901.
40. Ji, X.; Lee, K. T.; Nazar, L. F. A Highly Ordered Nanostructured Carbon–Sulphur Cathode for Lithium–Sulphur Batteries. *Nat. Mater.* **2009**, *8*, 500–506.
41. Diao, Y.; Xie, K.; Xiong, S.; Hong, X. Shuttle Phenomenon–The Irreversible Oxidation Mechanism of Sulfur Active Material in Li–S Battery. *J. Power Sources* **2013**, *235*, 181–186.
42. Brückner, J.; Thieme, S.; Böttger-Hiller, F.; Bauer, I.; Grossmann, H. T.; Strubel, P.; Althues, H.; Spange, S.; Kaskel, S. Carbon-Based Anodes for Lithium Sulfur Full Cells with High Cycle Stability. *Adv. Funct. Mater.* **2013**, *24*, 1284–1289.
43. Lee, S.-K.; Oh, S.-M.; Park, E.; Scrosati, B.; Hassoun, J.; Park, M.-S.; Kim, Y.-J.; Kim, H.; Belharouak, I.; Sun, Y.-K. Highly Cyclable Lithium-Sulfur Batteries with a Dual-Type Sulfur Cathode and a Lithiated Si/SiO_x Nanosphere Anode. *Nano Lett.* **2015**, *15*, 2863–2868.
44. Werner, J. G.; Johnson, S. S.; Vijay, V.; Wiesner, U. Carbon–Sulfur Composites from Cylindrical and Gyroidal Mesoporous Carbons with Tunable Properties in Lithium–Sulfur Batteries. *Chem. Mater.* **2015**, *27*, 3349–3357.
45. Ji, X.; Lee, K. T.; Nazar, L. F. A Highly Ordered Nanostructured Carbon-Sulphur Cathode for Lithium-Sulphur Batteries. *Nat. Mater.* **2009**, *8*, 500–506.
46. Zheng, G.; Zhang, Q.; Cha, J. J.; Yang, Y.; Li, W.; Seh, Z. W.; Cui, Y. Amphiphilic Surface Modification of Hollow Carbon Nanofibers for Improved Cycle Life of Lithium Sulfur Batteries. *Nano Lett.* **2013**, *13*, 1265–1270.
47. Zhang, W.; Qiao, D.; Pan, J.; Cao, Y.; Yang, H.; Ai, X. A Li^+-Conductive Microporous Carbon–Sulfur Composite for Li-S Batteries. *Electrochim. Acta* **2013**, *87*, 497–502.
48. Xin, S.; Gu, L.; Zhao, N. H.; Yin, Y. X.; Zhou, L. J.; Guo, Y. G.; Wan, L. J. Smaller Sulfur Molecules Promise Better Lithium-Sulfur Batteries. *J. Am. Chem. Soc.* **2012**, *134*, 18510–18513.
49. Wei Seh, Z.; Li, W.; Cha, J. J.; Zheng, G.; Yang, Y.; McDowell, M. T.; Hsu, P.-C.; Cui, Y. Sulphur–TiO_2 Yolk–Shell Nanoarchitecture with Internal Void Space for Long-Cycle Lithium–Sulphur Batteries. *Nat. Commun.* **2013**, *4*, 1331.
50. Ji, X.; Evers, S.; Black, R.; Nazar, L. F. Stabilizing Lithium–Sulphur Cathodes Using Polysulphide Reservoirs. *Nat. Commun.* **2011**, *2*, 325.